Geological Society of America
Special Paper 402
2006

The Lower Toluca Pumice: A ca. 21,700 yr B.P. Plinian eruption of Nevado de Toluca volcano, México

Lucia Capra
Lia María Carreras
Instituto de Geografía, Universidad Nacional Autónoma de México, México D.F., Mexico

José Luis Arce[†]
Instituto de Geología, Universidad Nacional Autónoma de México, México D.F., Mexico

José Luis Macías
Instituto de Geofísica, Universidad Nacional Autónoma de México, México D.F., Mexico

ABSTRACT

Approximately 21,700 yr B.P., after a period of quiescence of ~4800 yr, Nevado de Toluca volcano erupted, producing the Lower Toluca Pumice deposit. The activity generated a 24-km-high Plinian column that lasted ~11–13 h and dispersed 2.3 km^3 (0.8 km^3 dense rock equivalent) of tephra toward the NE, blanketing the Lerma basin, an area occupied today by the city of Toluca, with up to 5 cm of ash. Subsequent eruptive pulses were sub-Plinian in style, accompanied by phreatomagmatic explosions that emplaced surge deposits. Finally, the column collapsed toward the NE with the emplacement of a pumice flow deposit. The high vesicularity of the pumice from the basal Plinian layer, up to 83% by volume, indicates that exsolution was dominantly magmatic, and that pressurization of the magma chamber was probably due to a magma mixing process. Evidence for this includes the compositional range of juvenile products (61–65 wt% SiO_2), as well as the presence of two types of plagioclase, one in equilibrium and the other one with disequilibrium textures and reverse zoning. This suggests input of an andesitic liquid into the dacitic magma chamber. Based on the eruptive record, the most likely future eruptive activity at Nevado de Toluca volcano will be Plinian. Although quiet for more than 3250 yr, Plinian activity could occur after a long period of quiescence, and it could represent a hazard for the entire Toluca basin, where more than one million people live today.

Keywords: Plinian eruption, Nevado de Toluca, Trans-Mexican Volcanic Belt.

INTRODUCTION

Nevado de Toluca volcano (19°09′N, 99°45′W, 4680 m above sea level [masl]) is located in the central sector of the Trans-Mexican Volcanic Belt, 80 km southwest of Mexico City (Fig. 1). Activity at this andesitic to dacitic stratovolcano began ca. 2.6 Ma (De Beni, 2001; García-Palomo et al., 2002). Nevado de Toluca was built upon a complex sequence of metasedimentary and metavolcanic Jurassic rocks (Campa et al., 1974) of the Guerrero terrane (Centeno-García et al., 1993), a rhyolitic

[†]E-mail: jlarce@geologia.unam.mx.

Capra, L., Carreras, L.M., Arce, J.L., and Macías, J.L., 2006, The Lower Toluca Pumice: A ca. 21,700 yr B.P. Plinian eruption of Nevado de Toluca volcano, México, *in* Siebe, C., Macías, J.L., and Aguirre-Díaz, G.J., eds., Neogene-Quaternary continental margin volcanism: A perspective from México: Geological Society of America Special Paper 402, Penrose Conference Series, p. 155–173, doi: 10.1130/2006.2402(07). For permission to copy, contact editing@geosociety.org.

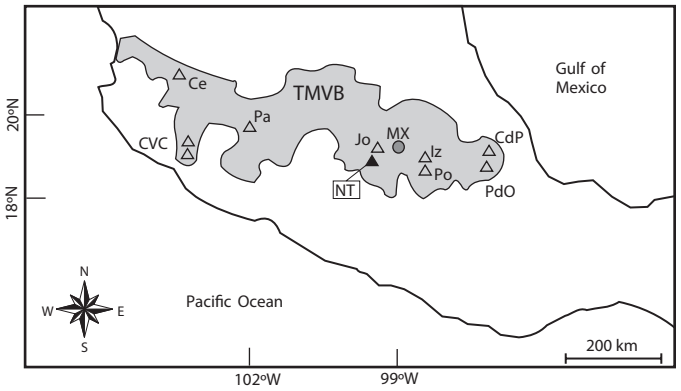

Figure 1. Sketch map of the Trans-Mexican Volcanic Belt (TMVB) showing the location of Nevado de Toluca (NT) volcano. Abbreviations are: Ce—Ceboruco; CVC—Colima volcanic complex; Pa—Parícutin; Jo—Jocotitlán; Iz—Iztaccíhuatl; Po—Popocatépetl; CdP—Cofre de Perote; PdO—Pico de Orizaba; MX—Mexico City.

ignimbrite sequence dated at 38.3 ± 1 Ma belonging to the Tilzapotla Formation (García-Palomo et al., 2002), and the 7.5 Ma Basal Sequence of andesitic lava flows, which represent some of the first episodes of the Trans-Mexican Volcanic Belt in this area (García-Palomo et al., 2002).

The present crater is elongated E-W (2 × 1.5 km) and holds the "Sun" and the "Moon" lakes, which are separated by a central dacitic dome called El Ombligo. This dome was emplaced after the 10,500 yr B.P. Plinian eruption that deposited the Upper Toluca Pumice (Bloomfield et al., 1977; Arce et al., 2003).

The volcano has been quiet since its last eruptive activity dated at 3250 yr B.P. (Macías et al., 1997), although minor fumarolic activity was reported during the nineteenth century (Bloomfield and Valastro, 1977). During the last 42 ka, the volcano has been characterized by different eruptive styles, including five dome collapses dated at 37, 32, 28, 26.5, and 14 ka (Macías et al., 1997; García-Palomo et al., 2002) and four Plinian eruptions at 36 ka (Ochre Pumice), 24.5 ka (Lower Toluca Pumice) (Bloomfield et al., 1977), 12.1 ka (Middle Toluca Pumice) (Arce et al., 2005), and 10.5 ka (Upper Toluca Pumice) (Macías et al., 1997; García-Palomo et al., 2002; Arce et al., 2003). All ages mentioned in this article are in ^{14}C yr B.P. The Upper Toluca Pumice represents the most violent and voluminous eruption, with the emission of 8 km^3 dense rock equivalent (D.R.E), and the formation of a 42-km-high Plinian column that dispersed material toward the ENE, blanketing the area occupied today by Mexico City with a >40-cm-thick pumice layer (Bloomfield et al., 1977; Arce et al., 2003).

Despite the extensive work dedicated to the geological aspects of the volcano (Bloomfield et al., 1977; Bloomfield and Valastro, 1974; Capra and Macías, 2000; García-Palomo et al., 2002; Macías et al., 1997), geomorphology (Heine, 1976; Norini et al., 2004) and pedostratigraphy (Sedov et al., 2001; Solleiro-Rebolledo et al., 2004), no attention has been dedicated to a detailed study of the Lower Toluca Pumice. Surprisingly, the Lower Toluca Pumice represents an anomalous event in the eruptive history of the volcano, because andesitic magma was erupted (in contrast to the predominantly dacitic composition of all other eruptions) and because of the presence of abundant exotic fragments from the metamorphic basement for which this deposit is easily recognizable.

In this work, we present new radiocarbon ages and detailed stratigraphic and sedimentological data for the Lower Toluca Pumice deposit, along with the interpretation of the eruptive chronology. In addition, we provide new petrographic and geochemical data of juvenile products to understand the eruptive style and the magmatic processes that triggered this eruption.

STRATIGRAPHY AND SEDIMENTOLOGY

A total of twenty sections have been studied to determine vertical and lateral variations of the Lower Toluca Pumice deposit (Table 1; Figs. 2 and 3). The most complete sequence is at section NT01 (133 cm thick) located 14.7 km NE from the crater, where most of the thirty-five samples representing all horizons of the Lower Toluca Pumice were collected, dry-sieved for fractions between –4ϕ (16 mm) and 4ϕ (0.0625 mm) (ϕ = –log$_2$ d, where d is the diameter measured in mm) (Fig. 4). Cumulative frequency curves define grain size (after Folk, 1980).

At section NT01, the sequence consists of eight horizons of intercalated fall and flow deposits, from bottom to top: PFD1, PFD2, SD1, PFD3, SD2, PFD4, SD3, PFD5, where PFD stands for pumice fall deposits and SD for surge deposits (Figs. 3 and 5).

TABLE 1. LOCATION OF TWENTY SELECTED SITES OF THE LOWER TOLUCA PUMICE DEPOSIT

Site	Latitude (°N)	Longitude (°W)	Thickness (cm)	Distance (km)
NT01	19°11′38″	99°39′03″	133	14.6
NT02	19°13′17″	99°42′03″	40	13.9
NT13	19°11′50″	99°41′38″	69	11.9
NT23	19°11′58″	99°42′18″	20.5	11.5
NT25	19°13′23″	99°40′32″	28	15.4
NT26	19°13′09″	99°42′09″	48	13.7
NT33	19°10′24″	99°43′31″	30	8.0
NT34	19°10′27″	99°43′26″	40	8.1
NT50	19°12′27″	99°39′22″	42	11.8
NT51	19°12′02″	99°37′49″	30	16.7
NT52	19°10′49″	99°37′09″	32	16.5
NT53	19°08′04″	99°41′01″	15	8.1
NT54	19°08′35″	99°39′25″	36	11.1
NT55	19°09′11″	99°36′54″	30	15.6
NT56	19°04′14″	99°39′20″	28	11.2
NT57	19°07′10″	99°40′54″	18	7.9
NT58	19°12′25″	99°43′08″	45	11.7
NT59	19°12′47″	99°43′20″	20	12.3
NT60	19°13′49″	99°43′40″	8	14.0
NT61	19°11′7″	99°39′48″	74.4	7.5

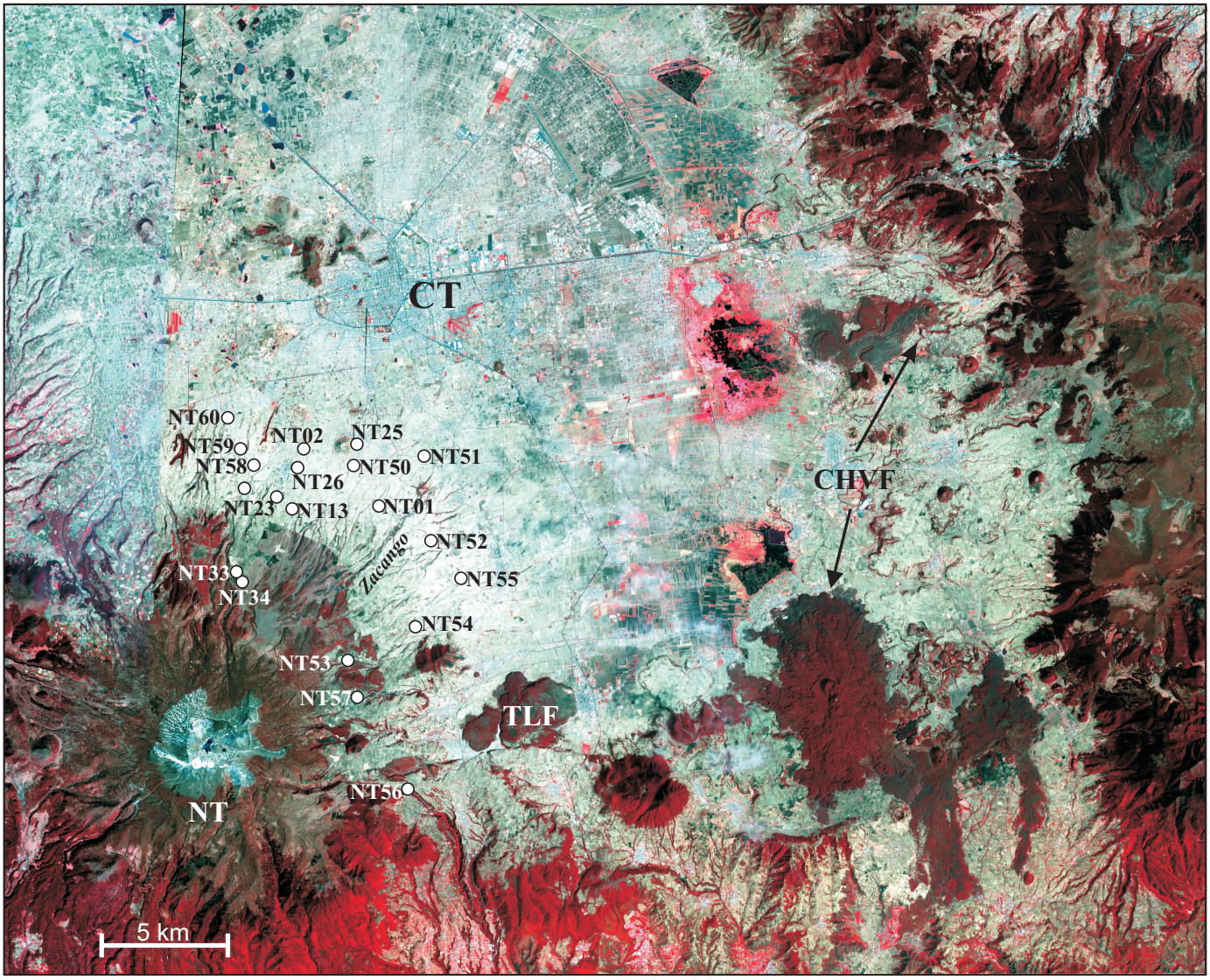

Figure 2. ASTER (Advanced Spaceborne Thermal Emission and Reflection Radiometer) satellite image (March 2001) of the Nevado de Toluca (NT) volcano and surrounding areas, showing the location of selected stratigraphic sections. Abbreviations are: TLF—Tenango lava flow; CT—city of Toluca; CHVF—Chichinautzin volcanic field. White dots stand for studied sites.

Extensive postdepositional remobilization of the nonwelded pyroclastic deposit has left few complete outcrops representative of the eruptive sequence. A pumice flow deposit (PFL-D) capped by an ash-fall layer (AFD) close the Lower Toluca Pumice sequence (Figs. 3 and 5).

The radial correlation of selected stratigraphic columns of the Lower Toluca Pumice (Figs. 2 and 3A, sections NT53, NT54, NT55) shows a gradual decrease of thickness with distance. The concentric correlation (Figs. 2 and 3B) between 11 and 15 km from the crater (sections NT58, NT13 and NT01, NT54) shows the main dispersal axis to be ~NE, as also observed from the isopach maps (Fig. 6A and 6B). Not all the Lower Toluca Pumice layers are homogeneously dispersed. As can be observed from sections in Figure 3, layers PFD2 and PFD3 are poorly distributed and are present only along the main dispersal axis, while PFD1, PFD4, and PFD5 are widely dispersed. Figures 3A and 3B show the correlation of selected stratigraphic sections. The Lower Toluca Pumice generally lies on top of a well-developed, black paleosol (PT2 of Sedov et al., 2001 and Solleiro-Rebolledo et al., 2004), while its upper limit is always marked by erosional surfaces capped by laharic horizons (Figs. 3A and 5B). As described in the following sections, textural characteristics and component contents have been used to make lateral correlations. In order to facilitate the deposit descriptions, maximum clast diameter is indicated in parenthesis after each component.

The PFD1 represents the basal layer, homogenously dispersed over the entire area, with a thickness that ranges from 14 cm at section NT55, to up to 82 cm at section NT01 along the

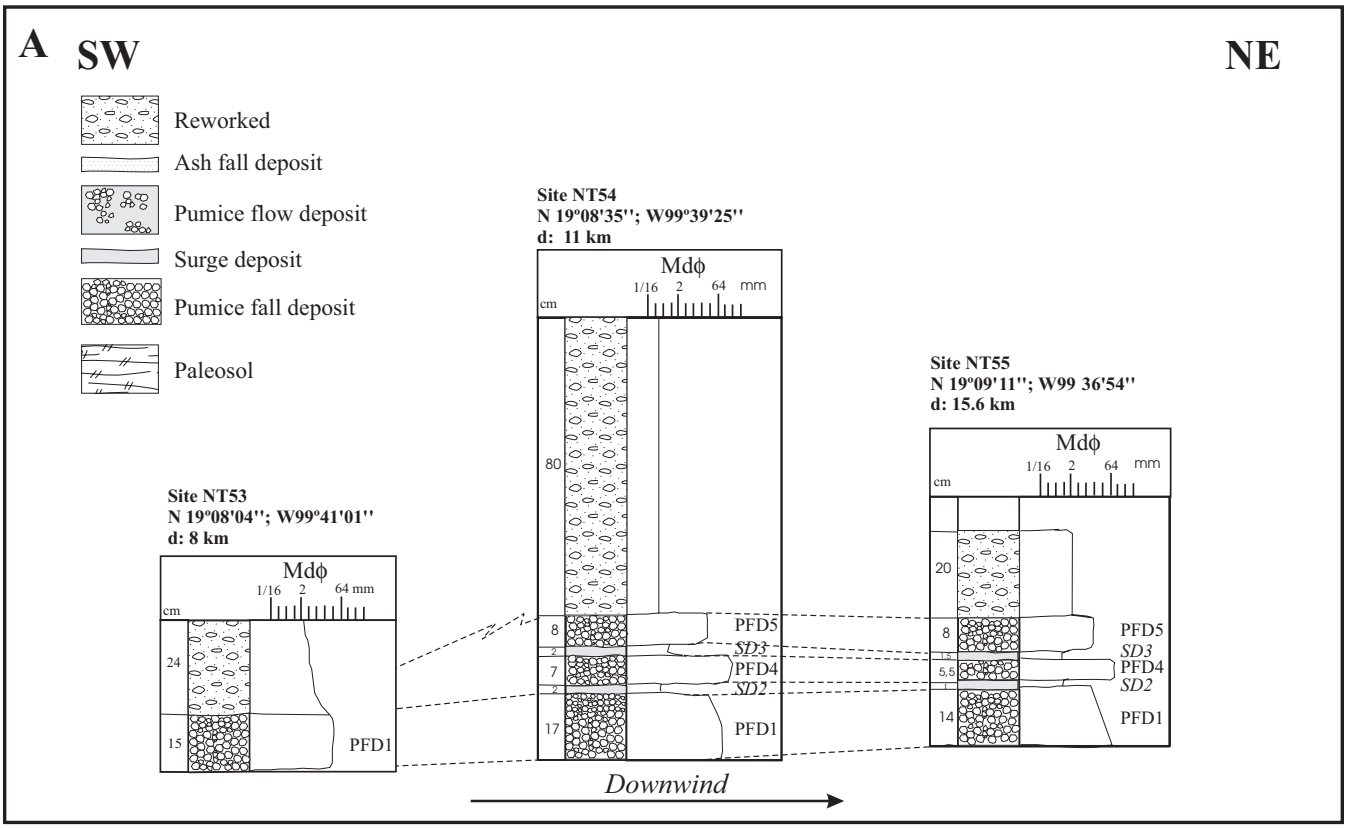

Figure 3. Stratigraphic correlation of the Lower Toluca Pumice for selected sections (A) downwind and (B) concentric with respect to the crater. For each stratigraphic column the mean grain size is represented by a graphic scale; d—distance from the vent; PFD—pumice fall deposits; SD—surge deposits; AFD—ash-fall layer.

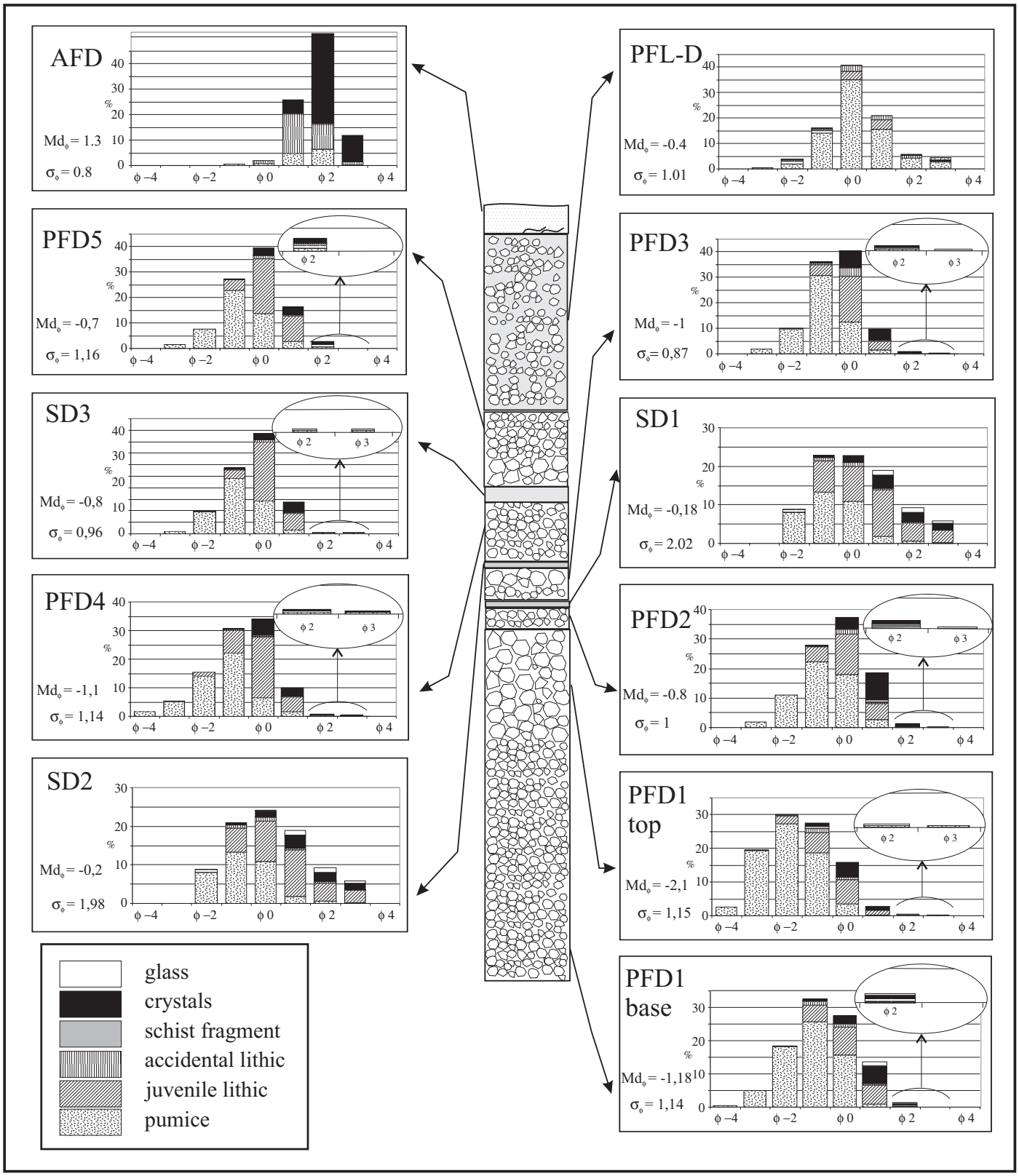

Figure 4. Histograms showing the granulometric and component characteristics of the Lower Toluca Pumice composite stratigraphic section. PFD—pumice fall deposits; SD—surge deposits; AFD—ash-fall layer.

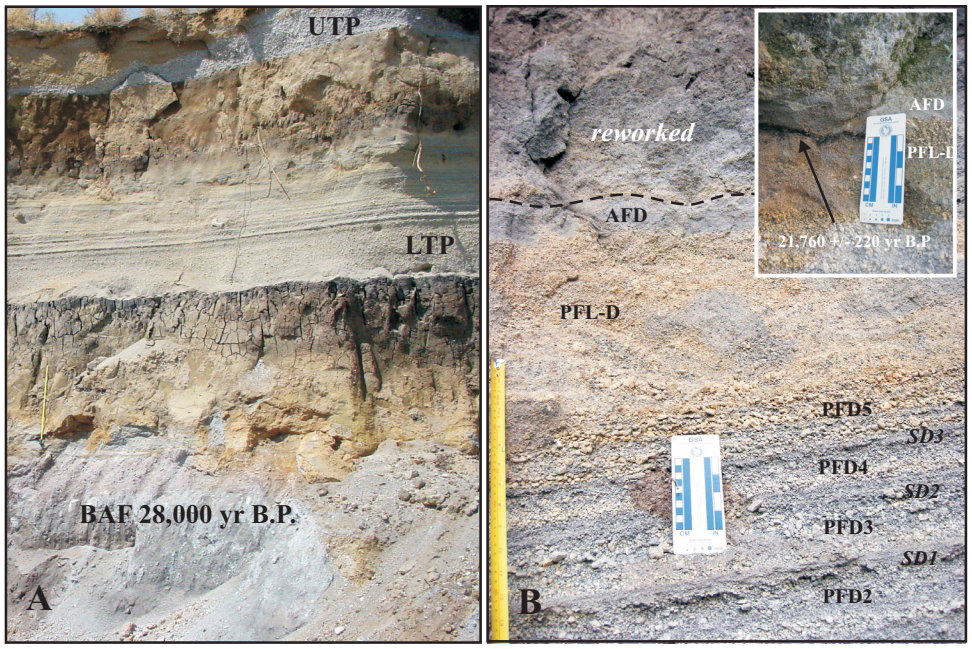

Figure 5. (A) View of section NT01 showing the stratigraphic relation of the Lower Toluca Pumice with respect to the 28,000 yr B.P. block-and-ash flow deposit (BAF) and the younger Upper Toluca Pumice fall deposit (UTP). Note the thick sequence of paleosols between these eruptive events that give evidence of long periods of repose. (B) Close-up of the upper sequence of the Lower Toluca Pumice deposit, showing the four fall horizons overlying surge layers. The fallout sequence is capped by a pumice flow deposit (PFL-D) and a lithic-rich ash-fall layer (AFD). The inset shows the location of charcoal found between these two layers that was dated at 21,760 ± 220 yr B.P.

main dispersal axis; both sections are ~14 km from the crater. This layer is clast-supported and, at the thickest sections (NT01 and NT13), reversely graded from sand and gravel at the base (Md_ϕ −1.18ϕ) to gravel toward the top (Md_ϕ −2.1ϕ). It is well sorted (σ_ϕ 1.14) and consists of ocher, subangular pumice clasts (up to 6 cm), and subangular lithic fragments (~1.5 cm), including low to incipiently vesicular, gray-colored fragments, with bread crust texture, (hereafter named juvenile lithics), and accidental fragments (red dacite and schist). Schist fragments represent an exclusive component of the Lower Toluca Pumice with respect to other fallout deposits of Nevado de Toluca volcano. These fragments were most likely derived from the Jurassic metamorphic rocks of the Guerrero terrane (Campa and Coney, 1983).

The sequence follows with two fall deposits, PFD2 and PFD3, separated by the SD1 surge layer, observable only at sections along the main dispersal axis (section NT01). PFD2 is a gray layer, 2.5 cm thick, massive, clast-supported, constituted by subangular, sand-sized ocher pumice (Md_ϕ −0.8ϕ), well sorted (σ_ϕ 1), with juvenile and accidental lithics (~0.6 cm). SD1 is massive, 2 cm thick, clast-supported, poorly sorted (σ_ϕ 2.02), with subrounded sand-sized pumice (Md_ϕ −0.18ϕ), and millimeter-sized accidental clasts. PFD3 is gray, 5 cm thick, clast-supported, reversely graded, sandy (Md_ϕ −1ϕ), well sorted (σ_ϕ 0.87), with subangular pumice (1.8 cm), and millimeter-sized accidental lithics.

The upper portion of the deposit ends with a sequence of two surge layers (SD2 and SD3) alternatively capped by two fall deposits (PFD4 and PFD5, Fig. 3A). Layer SD2 is laminated, varying in thickness from 1 to 3 cm, clast-supported, with sand-sized pumice (Md_ϕ −0.2ϕ), poorly sorted (σ_ϕ 1.98), and contains millimeter-sized accidental clasts. PFD4 varies in thickness from 9 to 5.5 cm, is massive, clast-supported, sandy to gravely (Md_ϕ −1.1ϕ), moderately sorted (σ_ϕ 1.14), with subangular ocher pumice (~3.1 cm), and angular lithic clasts (~1 cm). SD3 is a gray horizon, 1–2 cm in thickness, sandy (Md_ϕ −0.8ϕ), well sorted (σ_ϕ 0.96), with subrounded fragments of pumice (~1.8 cm), and lithics (up to 0.7 cm). PFD5 is an ocher layer, 8–9 cm thick, from massive to normal graded, clast-supported, sandy (Md_ϕ −0.7ϕ), moderately sorted (σ_ϕ 1.16), with subangular pumice (~2.3 cm), and accidental lithics (~1.5 cm).

The main fallout sequence is capped by the PFL-D layer, a pumice flow deposit, and the AFD horizon, an ash-fall layer, both well exposed along the Zacango barranca (Fig. 2). PFL-D is an ocher horizon, 28 cm thick, generally clast-supported, but with some matrix-enriched portions, massive, sandy (Md_ϕ −0.4ϕ) and well sorted (σ_ϕ 1.01), constituted by subrounded pumice fragments (~3 cm), and scarce accidental lithics (~0.5 cm). The AFD is a gray layer, with a homogeneous thickness of ~5 cm at a distance of 14 km from the crater, massive, fine sandy (Md_ϕ 1.3ϕ) and well-sorted (σ_ϕ 0.8), constituted by angular millimeter-sized accidental lithics and pumice. Charcoal and organic fragments were found at the base of this layer. We determined the age of the Lower Toluca Pumice for the first time by dating this material, as described next.

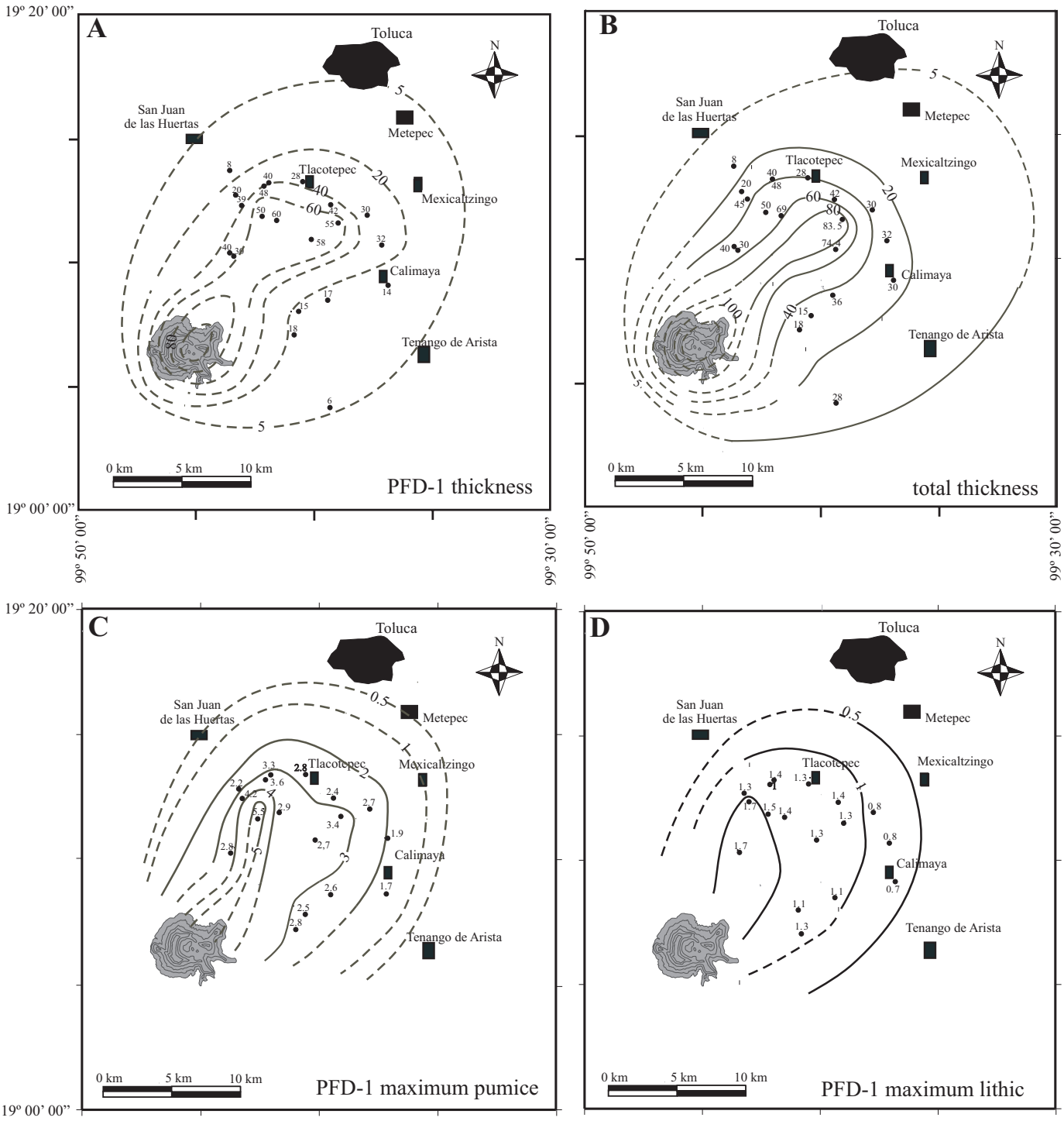

Figure 6. Isopach maps (in cm) for the (A) PFD1 horizon and (B) for the entire sequence. Isopleth maps (in cm) of the PFD1 layer for (C) pumice and (D) lithic fragments.

AGE OF THE EVENT

A paleosol underlying the Lower Toluca Pumice was first dated by Bloomfield and Valastro (1974, 1977) at 24,780 ± 250 yr B.P. (average of five ^{14}C dates), which represents the maximum age of the eruption. Two new radiocarbon dates were obtained in this work from paleosols at the base of the Lower Toluca Pumice, yielding ages of 24,940 +255/–245 yr B.P.,

18.7‰ $\delta^{13}C$, and 25,535 +340/–325 yr B.P., 18.6‰ $\delta^{13}C$, which are in good agreement with the first reported ages. We have dated the Lower Toluca Pumice more directly by sampling carbonized wood found at the base of the AFD, which is the topmost horizon of the Lower Toluca Pumice sequence. This yielded an age of 21,760 ± 220 yr B.P., 24.5‰ $\delta^{13}C$. Bloomfield and Valastro (1974) reported a similar age of 21,790 ± 200 yr B.P. by dating organic material found on sand and gravel layers on top of the Lower Toluca Pumice sequence but not correlated with the eruption by those authors. This new age for the Lower Toluca Pumice eruption lies between the two other documented Plinian eruptions dated at 36,000 (García-Palomo et al., 2002) and 10,500 yr B.P. (Arce et al., 2003), and suggests a rough recurrence interval of ~14–11 k.y. for Plinian events at Nevado de Toluca volcano.

COMPONENT ANALYSES

Component analyses were done on fractions from –4ϕ to 3ϕ (a minimum of 500 points were counted for each fraction). The results were plotted together with the granulometric histograms to show the variation in size distribution for the Lower Toluca Pumice composite section (Fig. 4), as well as vertical variations for each component (Fig. 7). The Lower Toluca Pumice components consist of pumice, gray juvenile lithics, red accidental dacite and schist fragments, crystals, and glass. All fall layers display a constant pumice content (~60%), while juvenile lithics gradually increase from base to top (from 20% to 30%), except for a slight decrease in the PFD2 layer (~20%). Content of the red dacite fragments is also constant, varying from 2% to 3%; in contrast, schist fragments are more abundant in layers PFD2, PFD3, and PFD5 (~2%) and scarce in the other layers (<1%). Finally, crystals increase from 15% to 20% from PFD1 to PFD2 and then gradually decrease to ~10%, whereas glass fragments suddenly decrease from PFD1 to PFD2 (from 4% to 2%) and then maintain a constant value (~1%). The surge layers differ in component content. Apparently, SD3 is very similar to the fall layers, whereas SD1 and SD2 are enriched in juvenile lithics, red dacite fragments, and glass (up to ~40%, ~4%, and ~5%, respec-

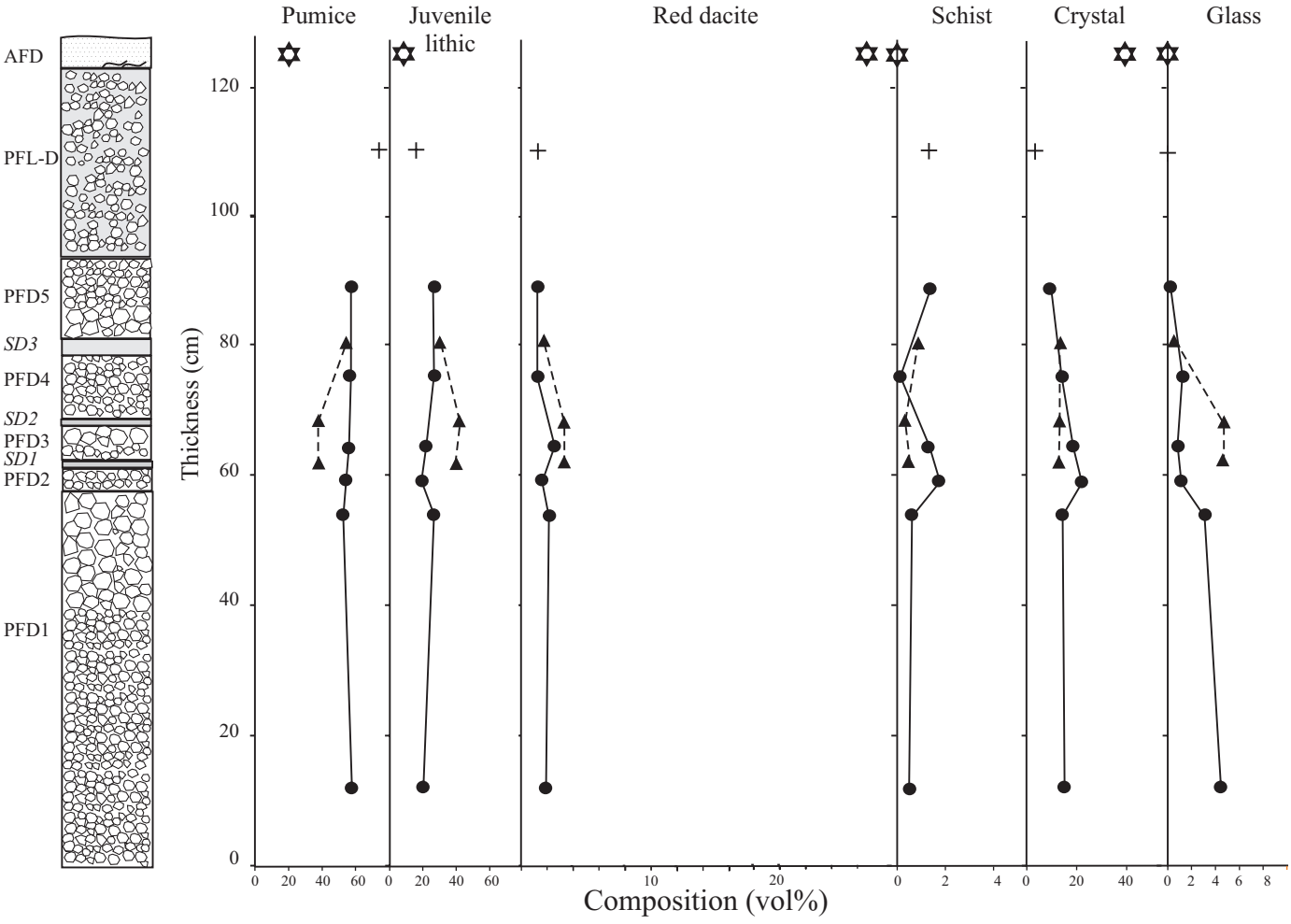

Figure 7. Vertical variation of component contents for the composite section of the Lower Toluca Pumice. Circles refer to fall, triangles to surge (SD), the cross to PFL-D (pumice flow), and the star to AFD (ash-fall) deposits.

tively) and depleted in pumice (~40%), schist fragments (<1%), and crystals (~15%).

VOLUME AND COLUMN HEIGHT

A total of 20 stratigraphic columns were used to construct the isopach and isopleth maps for the PFD1 layer of the Lower Toluca Pumice deposit (Figs. 6A, 6C, and 6D). The uppermost fall layers are always incomplete or absent from the stratigraphic sequence, precluding construction of isopach and isopleth maps, because they have been eroded by lahars, which left thick laharic deposits (Fig. 3B). For the same reason, we only estimated the volume and column height for the PFD1 layer, which is the thickest and most important fallout deposit of the Lower Toluca Pumice. Both isopach and isopleth maps show a main dispersal axis toward the NE (Figs. 6A, 6C, and 6D). The 5 cm isopach covers an area of ~520 km^2.

Minimum tephra volumes were calculated for the PFD1 layer using the isopach maps of Figure 6A, a linear regression plot of ln thickness versus area$^{1/2}$ (Fig. 8), and the expression as derived by Fierstein and Nathenson (1992). Since our data display only the proximal slope (Fig. 8), we used a theoretical value for the distal slope, as proposed by Carey et al. (1995) for proximal restricted data sets. Thus, we obtained a minimum tephra volume for the PFD1 of 2.1 km^3, considerably higher than the 0.25 km^3 previously estimated by Bloomfield et al. (1977). Considering an average tephra density of 1000 kg/m^3 and a magma density of 2500 kg/m^3, we estimated a D.R.E. volume of 0.85 km^3, which corresponds to an erupted mass of 2×10^{12} kg.

The isopleth map of PFD1 was constructed by using the average of the maximum diameter of the five largest lithic fragments in the layer (Fig. 6D), typically found in the middle part of the layer. By using the downwind range and crosswind range parameters of Carey and Sparks (1986), we estimated the maximum column height of the eruption that deposited PFD1 (Fig. 9). In this case, we used a clast diameter of 0.8 cm with a density of 2.5 g/cm^3, obtaining a column height of 24.5 km and a wind speed of 20 m/s. By comparing the thickness of PFD1 with the other fall horizons, we can qualitatively affirm that the other layers were emplaced from sub-Plinian eruptive columns with heights of less than 24 km, and probably even less than 20 km.

The maximum eruption column estimated previously can be converted to a maximum mass eruption rate according to the model of Sparks (1986). Assuming temperate atmospheric conditions and a magma temperature of 800 °C (see section below for temperature estimation), a maximum mass eruption rate of 4×10^7 kg/s was estimated for PFD1. By considering this mass eruption rate value and a mass of 2×10^{12} kg, we estimate a minimum duration time of 13 h for the Plinian column. A similar eruption duration was obtained by using the method proposed by Wilson and Hildreth (1997). Based on the average accumulation rate of 0.02 mm/s (from table 4 of Wilson and Hildreth, 1997) and the maximum observed thickness of 82 cm for the PFD1 layer, we obtained a duration time of 11.4 h.

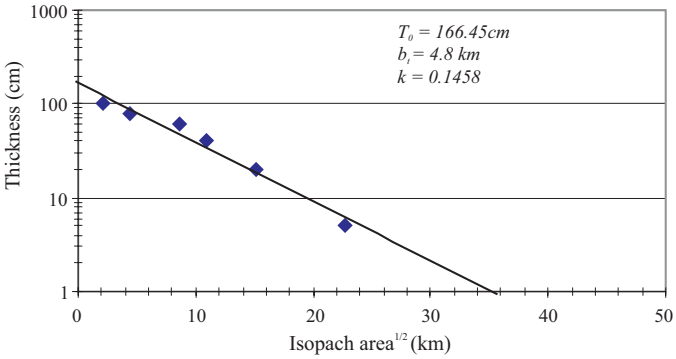

Figure 8. Thickness versus square root of the isopach area diagram for the PFD1 deposit. T_0, extrapolated maximum thickness; b_t, thickness half-distance, describing the rate of thinning of the deposit; k, slope of the line segment fitting the data with a single straight line.

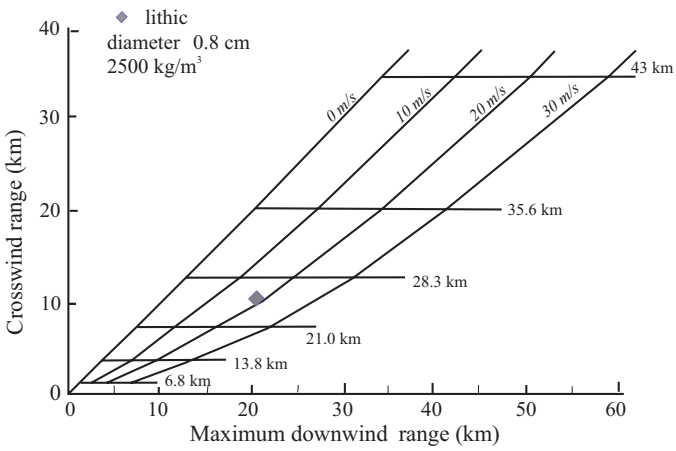

Figure 9. Diagram from Carey and Sparks (1986) showing a calculated column height of 24 km for the PFD1 layer

PUMICE VESICULARITY

Because vesicularity of pumice fragments provides valuable information on the vesiculation and fragmentation of the magma (Gardner et al., 1995; Houghton and Wilson, 1989; Sparks et al., 1978), we determined the vesicularity of pumice clasts within each fall layer. Using the methodologies of Gardner et al. (1995) and Houghton and Wilson (1989), we determined fragment densities (which were then converted to vesicularity) for a total of 150 pumice fragments ranging from 4 to 30 mm in diameter for each fallout. In particular, the vesicularity ranged between 70 and 83 vol% (Fig. 10). PFD1 was sampled at two levels (base and top), yielding vesicularities of 75 vol% at the base and 83 vol% at the top, similar to the values obtained for layer PFD2. In contrast, the vesicularity decreased to 70 vol% in layers PFD3 and PFD4, then increased to 75 vol% in layer PFD5. These data suggest that the eruption was probably driven by magmatic fragmentation, in agreement with vesicularity values proposed by previous

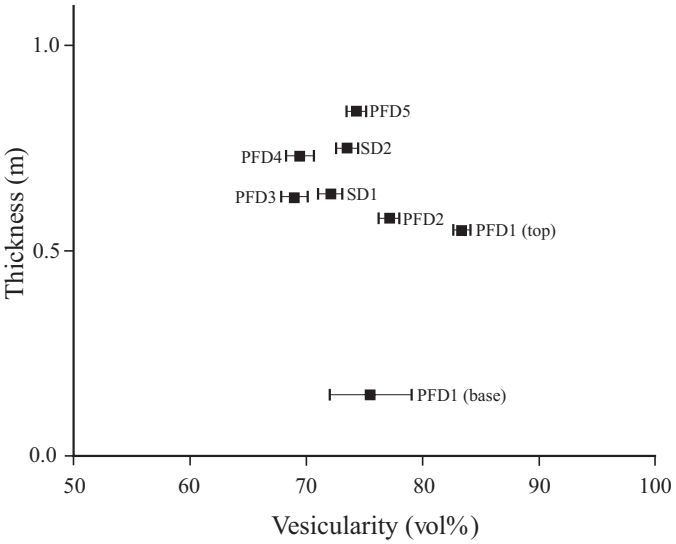

Figure 10. Diagram showing the vesicularity range determined for each layer of the Lower Toluca Pumice.

authors (Sparks et al., 1978; Houghton and Wilson, 1989). The observed decrease in the vesicularity toward the upper fall layers is in accordance with the model proposed by Wilson et al. (1995) and Houghton et al. (2004). This model indicates that with time the partially degassed magma builds up inward from the conduit walls, enhancing the reduction of the conduit and slowing the mass discharge rate. If water from the phreatic level is in contact with this stagnating magma, hydromagmatic explosions occur, producing small eruptive columns and fragmenting host rock that will be more abundant in the fallout deposits. The stratigraphy of the Lower Toluca Pumice clearly fits with this model; in fact the upper part of the sequence is characterized by the alternation of basal surges and fall deposits where schist fragments are more abundant than in the basal PFD1 layer.

PETROGRAPHY AND CHEMISTRY OF JUVENILE PRODUCTS

Five samples of juvenile material from the Lower Toluca Pumice were analyzed to determine their petrographic and geochemical characteristics. In particular, three pumice fragments and two highly vesiculated juvenile lithics were studied. The limited number of samples is due to the high degree of alteration of the deposit and to the reduced diameter of the fragments, which was generally smaller than 6 cm. Mineral and glass analyses were performed on the JEOL JXA-8600 electron microprobe at the CNR (Centro Nazionale di Ricerca) Università di Firenze (Italy).

We compared results from this work with those presented in previous studies of the Lower Toluca Pumice (Macías et al., 1997; Martínez-Serrano et al., 2004) and with other deposits, such as the Upper Toluca Pumice (Arce et al., 2003), block-and-ash flow deposits produced during the last 42,000 yr (D'Antonio et al., 2004), and samples from the Tenango lava flow (García-Palomo et al., 2002).

Petrography and Mineral Chemistry

Two pumice clasts from layer PFD1 (NT25, NT13A) and one from layer PFD4 (NT54C) show porphyritic-seriate textures, and similar mineral assemblages with plagioclase (Pl), hornblende (Hbl), apatite (Ap), and oxides set in a glassy matrix (up to 95 vol%). Two different types of plagioclase are present (Fig. 11): (1) subhedral crystals with maximum dimensions of 4 mm, always zoned and twinned (Carlsbad type), defined by dusty/cellular zones of glass inclusions as in a sieve-like texture; and (2) elongated euhedral prismatic crystals up to 1–2 mm with clear and uniform grain interiors that are sometimes twinned (Carlsbad type). Type 1-Pl displays reverse zoning varying from $An_{40–50}$ (core) to $An_{43–60}$ (rim), while type 2 shows a uniform composition similar to the rim of type 1-Pl, with $An_{50–58}$ (Table 2).

Hornblende varies from euhedral to subhedral in shape, is up to 2 mm long and barren of any type of alteration/oxidation (Fig. 12A). Chemically, hornblendes fall between the pargasite and edenite fields (Fig. 12B; Table 3). The glass in the matrix is rhyolitic, with a wide compositional range from 68 to 75 wt% SiO_2 (Table 4). Fe-Ti oxides (titanomagnetite and ilmenite) are present as a groundmass phase or as inclusions in hornblende (Table 5). Based on the ilmenite-titanomagnetite geothermometer (Andersen and Lindsley, 1988), a magma temperature of 837 ± 6 °C was obtained for the dacitic pumice (Table 5). A few quartz phenocrysts and fragments of sedimentary rocks are also hosted by the glass matrix (Fig. 13).

Juvenile lithics (NT01E and NT54C-1) have the same mineralogical paragenesis as the pumice, with, in order of abundance, Hbl, Pl, Ap, Fe-Ti oxides, and rare clinopyroxene, all set in a matrix of Pl microlites. Hornblende varies from euhedral to subhedral, is up to 2 mm long, and generally occurs as aggregates. Juvenile lithics do not show alteration, but do contain oxide and zircon crystals, as observed in the pumice fragments. The two types of plagioclase in the pumice, already described, are also present in the juvenile lithics, although type-2 Pl is scarce. Again, xenocrysts of quartz and sedimentary rocks (schists and recrystallized subgrains of quartz) are present as inclusions in the juvenile lithics (Fig. 13).

Whole-Rock Chemistry

Major, trace and rare earth elements were determined by inductively coupled plasma–mass spectrometry (ICP-MS) (Tables 6A and 6B) at Activation Laboratories, Ontario, Canada. The composition varies from andesite, found only in some pumice fragments (including data from Macías et al., 1997 and Martínez-Serrano et al., 2004) to dacite (pumice and lithic fragments). The samples belong to the calc-alkaline series (Fig. 14), and the SiO_2 content varies from 61 to 66 wt% (anhydrous basis). By comparing these data with Nevado de Toluca products younger

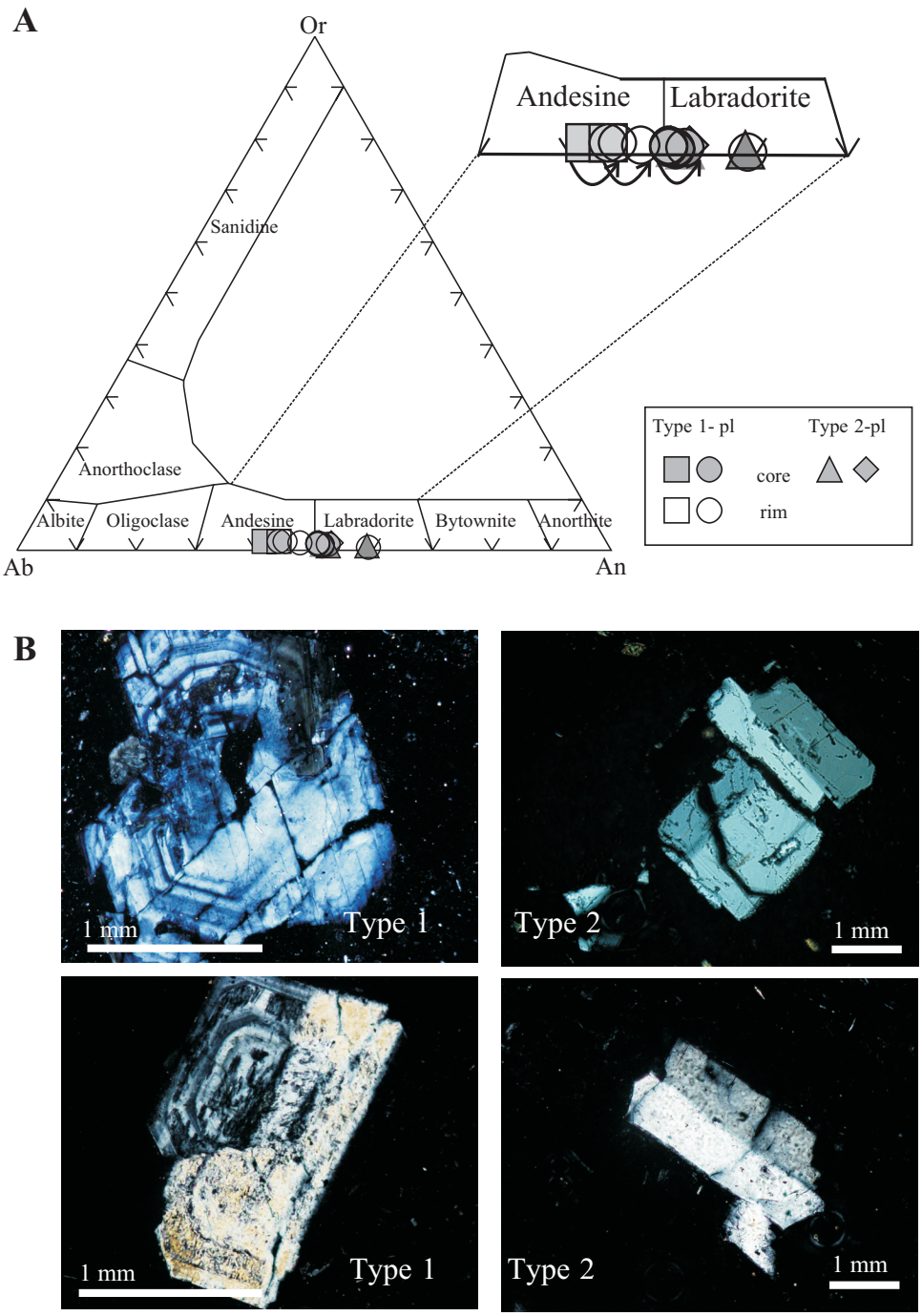

Figure 11. (A) Chemical composition of plagioclase. The curved arrows in the enlargement indicate the variation in composition from core to rim in a single crystal. (B) Photomicrographs of thin sections of plagioclase showing two types of phenocrysts.

than 42,000 yr, the Lower Toluca Pumice represents the most basic as well as the most differentiated product for a single event, with ~5 wt% of SiO_2 variation between juvenile components. In fact, block-and-ash flow deposits erupted during the past 42,000 yr are clearly dacitic, with SiO_2 contents between 65 and 67 wt%, including the Upper Toluca Pumice. Despite the small number of samples analyzed, the Harker diagrams (Fig. 15) show positive trends for the alkali elements, such as Na and K, as well as for Sr and Zr, and a relative decrease in Mg, Mn, Ca, Y, and V for the more differentiated samples.

TABLE 2. CHEMICAL COMPOSITION OF SELECTED PLAGIOCLASE CRYSTALS

Sample	SiO_2	TiO_2	Al_2O_3	FeO*	MnO	MgO	CaO	Na_2O	K_2O	Total	Ab	An	Or
Mcplg2	57.5	0.01	27.89	0.25	0.08	0	9.51	5.06	0.26	100.56	48.3	50.1	1.6
Mcplg3	57.49	0.06	28.64	0.23	0	0	9.84	4.82	0.24	101.32	46.3	52.2	1.5
Mc-1	53.57	0.04	29.73	0.29	0	0	11.75	4.51	0.17	100.06	40.6	58.4	1
Mc-2	55.69	0.02	28.37	0.37	0.06	0	10.17	5.33	0.2	100.21	48.1	50.7	1.2
Mc-3	56.4	0	28.63	0.25	0.02	0.06	10.24	5.12	0.18	100.9	47	51.9	1.1
Phc2-c	60.24	0	26.72	0.1	0.01	0	7.66	6	0.27	101	57.6	40.7	1.7
Phc2-r	59.77	0	26.52	0.17	0	0.01	7.82	5.51	0.27	100.07	55	43.2	1.8
Phcplg1	52.73	0.08	29.7	0.41	0	0.11	12.06	4.06	0.36	99.51	37	60.8	2.2
Phcplg3-c	59.6	0	27.31	0.15	0.02	0	8.22	5.78	0.27	101.35	55	43.3	1.7
Phcplg3-r	56.7	0.04	28.85	0.13	0	0	10.03	5.22	0.21	101.18	47.9	50.9	1.3
Phcplg3-rr	59.27	0	27.07	0.17	0.01	0	8.26	5.6	0.28	100.66	54.1	44.1	1.8
Phcplg3-rrr	55.92	0.06	28.68	0.17	0.02	0.02	10.01	5.22	0.18	100.28	48	50.9	1.1
Phcplg4-c	57.49	0	27.58	0.16	0	0	8.85	4.74	0.22	99.04	48.5	50	1.5
Phcplg4-r	57.37	0.04	27.65	0.22	0.05	0.03	8.86	5.38	0.23	99.83	51.6	46.9	1.5
Phcplg5-r	55.23	0.07	29.43	0.29	0	0.04	11.27	4.28	0.12	100.73	40.4	58.8	0.7
Phcplg6-r	56.68	0.05	28.4	0.07	0	0	10.03	5.05	0.19	100.47	47.1	51.7	1.2
Phcplg7-r	56.49	0	28.21	0.34	0	0	9.8	5.29	0.22	100.35	48.8	49.9	1.3

Note: Abbreviations are: Mc—microcrysts; Phc—Phenocrysts; Ab—albite; An—anorthosite; Or—orthoclase.
*Total Fe as FeO.
Analytical conditions: acceleration potential = 15 kV; beam current = 15 nA; counting time 15–20 s, with a focused beam. The data were corrected for matrix effects using the method of Bence and Albee (1968).

DISCUSSION: ERUPTIVE HISTORY OF THE LOWER TOLUCA PUMICE

Based on the stratigraphic record of the Lower Toluca Pumice, it is possible to reconstruct the chronology of this Plinian eruption of the Nevado de Toluca volcano. Just prior to the eruption, ca. 21,700 yr B.P., the Nevado de Toluca volcano most likely had a morphology with a crater similar to its present crater, but without a central dome. This suggestion is supported by the lack of block-and-ash flow deposits or lithic-rich layers at the base of the Lower Toluca Pumice fallout sequence that would have indicated a dome destruction stage prior to Plinian activity. By inference, when the Lower Toluca Pumice eruption started, the volcano had an open conduit that allowed the establishment of a 24-km-high Plinian column, which dispersed ejecta northeastward for ~11–13 h. The plume blanketed the Lerma basin with up to 5 cm of pumice over an area occupied today by the city of Toluca (more than 1 million inhabitants). The reverse grading of the basal fall layer (PFD1), as well as the vesicularity index that increases from 75% to 83% through the layer suggest that the energy of the eruptive column was augmented. At least four other pulses are recorded in the stratigraphic record of the Lower Toluca Pumice, but, as discussed before, they were emplaced from sub-Plinian columns (<20 km high), and were probably accompanied by phreatomagmatic explosions, as evidenced by the presence of base surge layers at the bottom of each fall horizon. This phreatomagmatic component is only documentable for the final stage of the PFD1 eruption. In fact, despite the lack of any surge deposit at the base of the sequence, the high vesicularity of pumice in layer PFD1 (~83 vol%) indicates that vesiculation drove magma fragmentation (Sparks et al., 1978; Houghton and Wilson, 1989). At the very end of the eruption, the column collapsed toward the NE and emplaced a pumice flow deposit (PFL-D). The upper lithic- and crystal-rich ash fallout (AFD) probably represents a final phreatic pulse.

Based on the chemical data presented here, it is difficult to determine the process that initiated the Plinian eruption. The vesicularity index excludes a phreatomagmatic component as the triggering process for the Plinian phase. Instead, a shift in pressure or temperature of the magma in the chamber would be required to explain the eruptive trigger mechanism. Two characteristics of the petrographic and mineral chemistry of the juvenile products suggest magma mixing: (1) the occurrence of two types of plagioclase phenocrysts, one of which was unstable and is reversely zoned (type 1), and the other type (type 2) that was in equilibrium, with a composition similar to that of the rim of the unstable type-1 Pl (Fig. 11), and (2) the relatively wide range of SiO_2 (5 wt%) in the juvenile products (Fig. 14). This evidence suggests that a more basic magma (with a SiO_2 content of at least 61 wt%, similar to the more basic pumices) intruded into a dacitic magma chamber (SiO_2 of 66 wt%). Subsequent magma mixing caused temperature variations and crystal disequilibrium, creating a new gas-rich hybrid magma that equilibrated prior to the eruption at 837 ± 6 °C (as suggested by the Fe-Ti oxide temperatures). The source of the basic magma can be related to the magmatic system feeding the Chichinautzin volcanic field during the last 40,000 yr (Bloomfield, 1975; Siebe et al., 2004). In fact, the Y/Rb versus Rb and the La/Rb versus 1/Rb ratios for samples from the Tenango andesitic lava flow (data from García-Palomo et al., 2002) and the more differentiated Lower Toluca Pumice juvenile products follow a regression line (mixing) along which all the intermediate products lie (Fig. 16). We chose the Tenango lava flow as an end-member composition, because it lies in the vicinity of the Nevado de Toluca volcano (Fig. 2). We note that, based on the eruptive history described by Macías et al. (1997), during the past 42 k.y., the Nevado de Toluca volcano changed

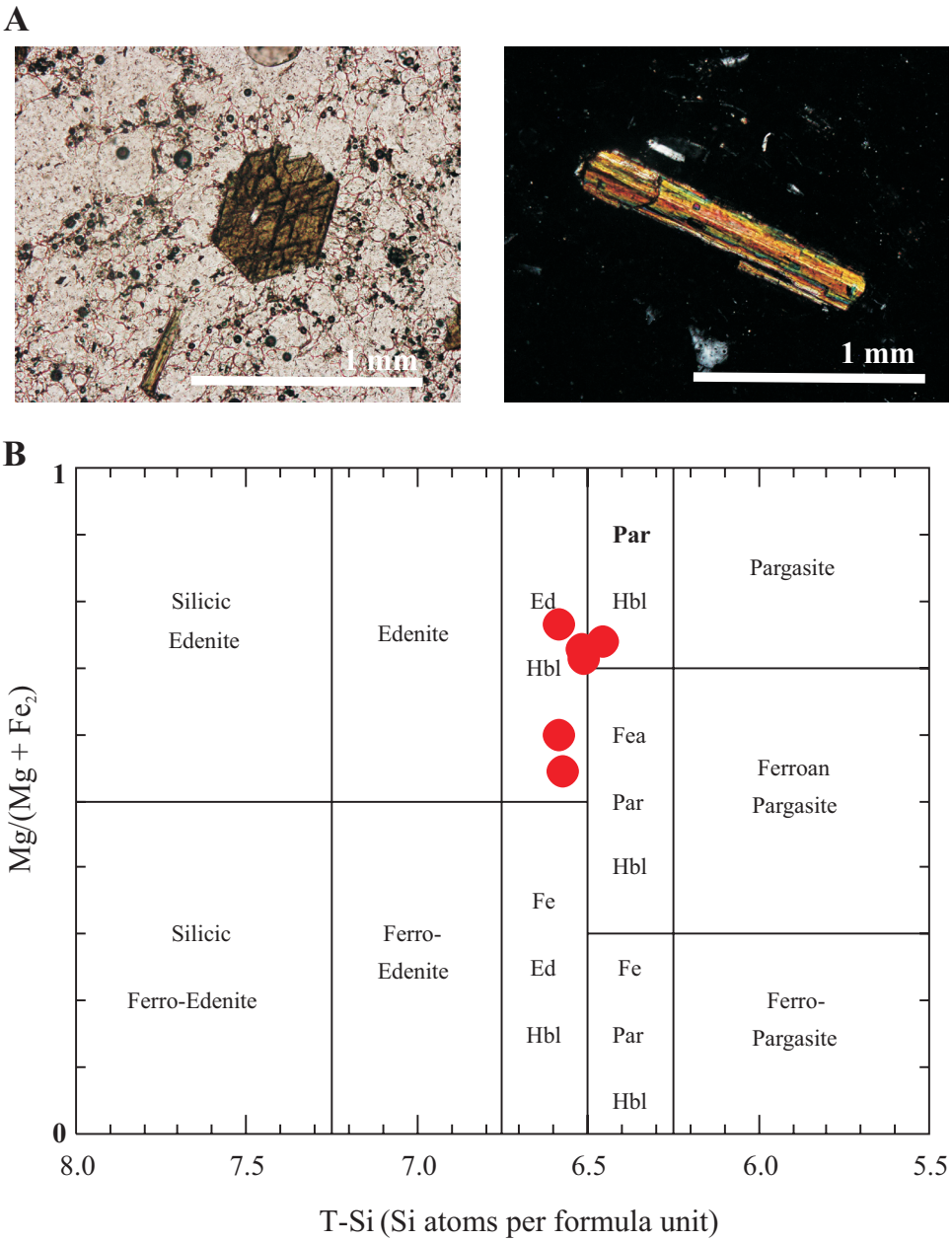

Figure 12. (A) Photomicrographs of thin sections of hornblende (Hbl) crystals (plane-polarized and cross-polarized light). (B) Chemical composition of hornblende.

TABLE 3. CHEMICAL COMPOSITION OF HORNBLENDE.

Sample	SiO_2	TiO_2	Al_2O_3	FeO*	Cr_2O_3	MnO	MgO	CaO	Na_2O	K_2O	Total
Mc-hb3	45.23	1.82	10.39	15.55	0.03	0.27	13.1	10.51	2.19	0.44	99.53
Phc-hb1	45.98	1.93	10.29	9.31	0.03	0.21	16.92	11.3	2.03	0.42	98.42
Phc-hb2	44.43	1.55	10.23	18.15	0	0.34	12.16	9.74	1.94	0.32	98.86
Phc-hb4	45.07	2.06	10.65	10.68	0.02	0.13	15.93	11.16	1.95	0.45	98.1
Phc-hb5	44.77	2.1	11.63	9.93	0.08	0.07	15.86	11.02	2.09	0.48	98.03
Phc-hb6	45.25	2.12	11.06	11.16	0.04	0.17	15.54	10.89	1.93	0.48	98.64

Note: Abbreviations are: Mc—microcrysts; Phc—Phenocrysts; *Total Fe as FeO. Analytical conditions: acceleration potential = 15 kV; beam current = 15 nA; counting time 15–20 s, with a focused beam. The data were corrected for matrix effects using the method of Bence and Albee (1968).

TABLE 4. CHEMICAL COMPOSITION OF GLASS

Sample	SiO_2	TiO_2	Al_2O_3	FeO*	MnO	MgO	CaO	Na_2O	K_2O	Total
Gl-2	72.21	0.33	15.46	2.17	0.04	0.46	2.07	4.33	2.92	97.21
Gl-3	75.35	0.28	15.71	2.29	0.00	0.42	2.06	1.90	2.00	95.36
Gl-4	70.17	0.26	17.20	1.79	0.03	0.43	3.09	4.69	2.34	97.35
Gl-5	74.50	0.24	14.54	2.31	0.02	0.35	2.21	3.45	2.35	95.26
Gl-6	72.94	0.38	14.80	2.67	0.06	0.75	1.94	3.66	2.80	97.96
Gl-7	74.23	0.34	16.00	2.55	0.05	0.46	2.19	2.00	2.16	94.19
Gl-8	68.66	0.29	18.16	1.99	0.07	0.47	3.58	4.72	2.06	97.29
Gl-9	72.64	0.31	15.24	2.16	0.11	0.53	1.87	4.32	2.81	96.57

Note: *Total Fe as FeO. Analytical conditions: acceleration potential = 15 kV; beam current = 15 nA; counting time 15–20 s, with a defocused beam of 10–15 µm in diameter. The data were corrected for matrix effects using the method of Bence and Albee (1968).

from dominantly effusive to explosive activity contemporaneously with the formation of scoria cones and fissural lava flows of the Chichinautzin volcanic field. This could suggest that the enhancing process of the younger explosive activity was a mixing process between these two different magma sources, as proposed here for the Lower Toluca Pumice.

As mentioned before, one of the most peculiar characteristics of the Lower Toluca Pumice deposit is the presence of schist fragments from the basement rocks, so far not found in other pyroclastic deposits of the Nevado de Toluca volcano (Fig. 13), and more abundant in the upper fall layers PFD3, PFD4, and PFD5. These layers were associated with the final hydromagmatic pulses, which, as suggested by Houghton et al. (2004), could have favored explosion in the conduit and the introduction of wall rock fragments. In addition, schist fragments without resorption features have been found as inclusions in the pumice, indicating a rapid expulsion (Fig. 13A–B).

HAZARD ASSESSMENT

The Nevado de Toluca volcano is considered to be a quiescent active volcano, since its last activity occurred 3250 yr B.P. (Macías et al., 1997). However, the Upper Toluca Pumice Plinian eruption, which represents one of the most violent eruptions in America since the late Pleistocene, occurred at only 10,500 yr B.P. (Macías et al., 1997; Arce et al., 2003). Based on the stratigraphic reconstruction proposed by Macías et al. (1997), the time interval between different eruptive periods varies from a minimum of 1.6 k.y. (e.g., between the 10,500 yr B.P. Upper Toluca Pumice and the 12,100 yr B.P. Middle Toluca Pumice; Arce et al., 2005) to a maximum of 8.7 k.y. (e.g., between the ca. 21,700 yr B.P. Lower Toluca Pumice and the ca. 13,000 yr B.P. block-and-ash flow deposit), and, in particular, a period of ~11–14 k.y. seems to be the recurrence time between Plinian eruptions (the 36,000 yr B.P. Ochre Pumice, the ca. 21,700 yr B.P. Lower Toluca Pumice, and the 10,500 yr B.P. Upper Toluca Pumice). At present, the crater of Nevado de Toluca is filled by the small, 50-m-high El Ombligo dome, the maximum height of which does not reach the elevation of the crater rim. Considering the time interval between eruptions, a recurrence of Plinian activity represents the most probable future eruptive scenario. In the case of a new Plinian eruption, it is likely that the Lerma basin would be covered by at least 5 cm of pumice, significantly affecting human activity in the city of Toluca.

CONCLUSIONS

Approximately 21,700 yr B.P., after a quiescence period of 4.8 k.y., the Lower Toluca Pumice Plinian eruption occurred at Nevado de Toluca volcano. The activity generated at least five eruption columns, the first of which reached an altitude of 24 km and was dispersed toward the NE. It produced 2.1 km^3 of tephra (0.8 km^3 D.R.E.) deposited over an area of 520 km^2. Subsequent pulses were sub-Plinian, each initiated by a phreatomagmatic component, which emplaced surge deposits. Finally, the column collapsed toward the NE. Petrographic and chemical evidence suggests a magma mixing process as the triggering mechanism for the initial Plinian eruption, with the injection of andesitic magma (~61 wt% SiO_2) into a dacitic (~66 wt% SiO_2) chamber. Based on the eruptive record of Nevado de Toluca volcano, reactivation of Plinian activity is the most likely potential scenario in the future. The volcano has been quiet since ca. 3.2 ka, but, as shown by the Lower Toluca Pumice stratigraphic record, where the main eruptive pulse lies directly on top of a thick paleosol, a Plinian eruption could occur after long periods of inactivity. If this were to happen, it would represent a significant hazard for the entire Lerma basin, where more than 1 million people live.

TABLE 5. CHEMICAL COMPOSITION OF Fe-Ti OXIDES AND TEMPERATURE CALCULATED ACCORDING TO THE ANDERSEN AND LINDSLEY (1988) MODEL

Sample	SiO_2	TiO_2	Al_2O_3	Cr_2O_3	FeO*	MnO	MgO	CaO	Na_2O	K_2O	Total	XIlm	XUsp	T°C	fO_2
Ilm1	0.04	44.53	0.28	0	51.13	0.52	2.83	0.11	0.13	0	99.58	0.805		843	–12.013
Ilm2	0	43.9	0.3	0	49.83	0.36	2.96	0.19	0	0.02	97.56	0.809		833	–12.174
Ilm3	0.06	43.89	0.4	0.06	50.38	0.49	2.88	0.08	0	0	98.24	0.804		843	–12.008
Ilm4	0.07	44.12	0.3	0.06	49.9	0.46	2.83	0.04	0.13	0	97.92	0.813		836	–12.183
Ilm5	0.03	44.4	0.31	0	49.82	0.45	2.92	0.05	0.06	0	98.03	0.815		833	–12.253
Tmgt1	0.02	9.9	3.34	0.18	78.17	0.34	1.96	0.06	0.16	0.04	94.18		0.276		
Tmgt2	0.15	10.34	3.26	0.17	80.11	0.3	1.71	0.08	0.09	0	96.2		0.289		

Note: Abbreviations are: Ilm—Ilmenite; Tmgt—titanomagnetite; XIlm—molar fraction of ilmenite in ilmenite; XUsp—molar fraction of titanomagnetite in magnetite. Analytical conditions: acceleration potential = 15 kV; beam current = 15 nA; counting time 15–20 s, with a focused beam. The data were corrected for matrix effects using the method of Bence and Albee (1968).

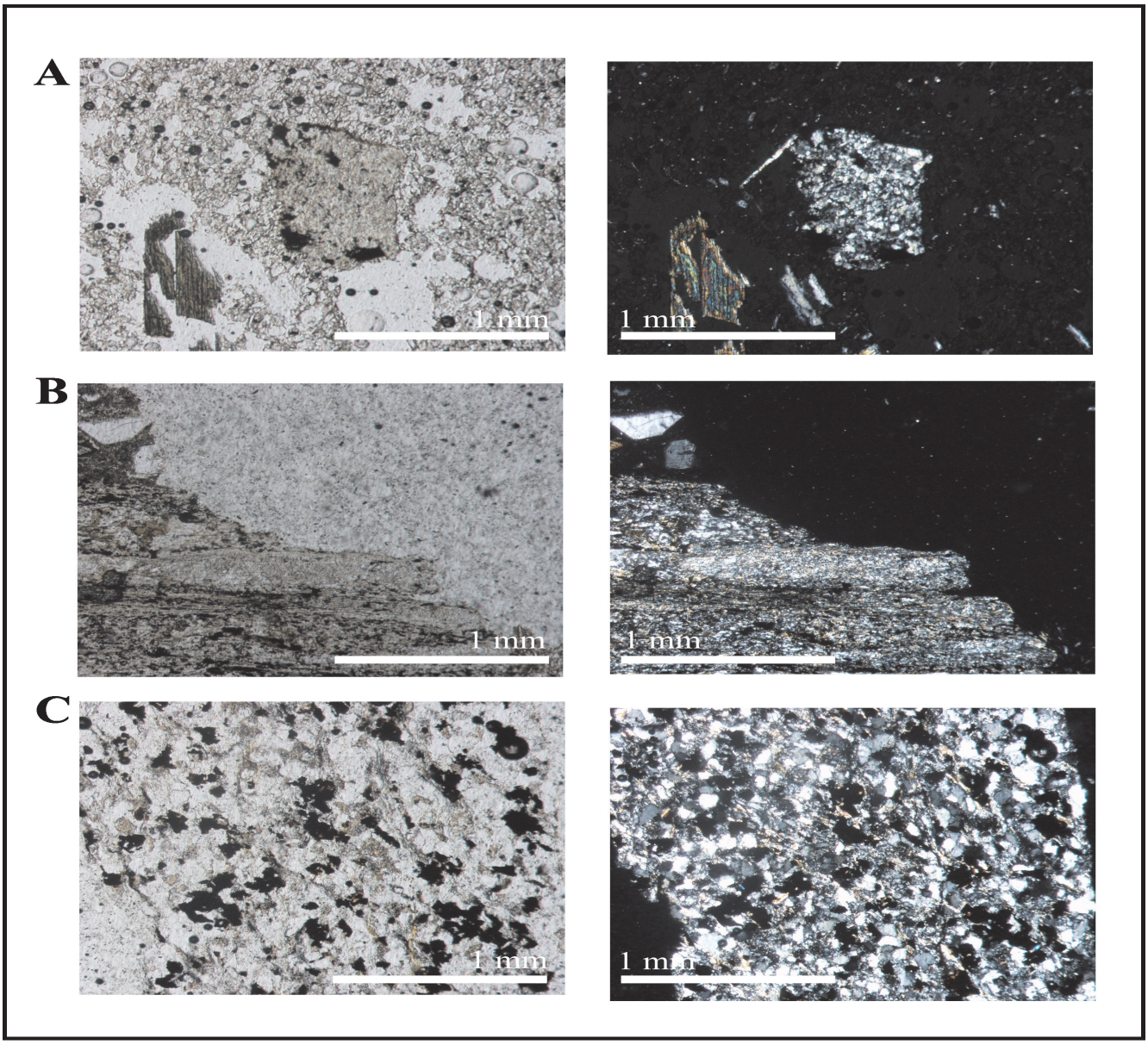

Figure 13. Photomicrographs of thin sections of accidental lithics (plane-polarized and cross-polarized light): (A) quartz fragment in pumice; (B) schist fragment in pumice; (C) fragment of recrystallized subgrains of quartz isolated from the matrix.

TABLE 6A. MAJOR ELEMENT ANALYSES OF THE LOWER TOLUCA PUMICE AND JUVENILE LITHICS

Sample	SiO_2	Al_2O_3	Fe_2O_3tot	MnO	MgO	CaO	Na_2O	K_2O	TiO_2	P_2O_5	Total	LOI	Total2
NT13A	64.15	17.81	5.03	0.07	1.96	4.38	4.00	1.73	0.65	0.20	100	4.78	99.93
NT54C	64.16	17.87	4.70	0.07	2.03	4.50	4.17	1.61	0.69	0.20	100	4.26	99.76
NT25	65.37	16.94	4.20	0.07	1.95	4.25	4.37	2.03	0.65	0.16	100	3.52	100.71
NT54o	64.69	16.44	5.16	0.08	2.22	4.37	4.33	1.93	0.64	0.16	100	1.59	99.11
NT01E	66.32	15.94	4.86	0.07	1.93	4.04	4.26	1.79	0.62	0.16	100	1.35	99.44
NT8-AP†	61.05	20.42	5.29	0.05	2.28	4.88	3.63	1.41	0.75	0.23	100	8.79	99.86
NT33-D†	64.94	17.70	4.20	0.06	1.78	4.24	4.34	1.86	0.67	0.21	100	4.21	99.74
NT9562‡	61.19	20.50	5.49	0.10	2.16	4.70	3.51	1.38	0.75	0.21	100	8.22	98.57

Note: LOI: loss on ignition at 925 °C. Total2, unnormalized sum including LOI.

†Sample from Martinez-Serrano et al. (2004).

‡Sample from Macías et al. (1997). Oxides analyzed by fusion ICP-MS in wt%. Data have been normalized to 100% on an anhydrous basis.

TABLE 6B. TRACE ELEMENT ANALYSES
OF THE LOWER TOLUCA PUMICE IN PPM

Sample	NT13A	NT54C	NT54o	NT01E	NT01
Sc	8	9	9	8	18
V	56.34	58.48	59.97	57.91	135.58
Cr	45.96	37.93	63.41	47.35	160.50
Cu	13.90	14.61	14.26	10.00	19.56
Zn	49.95	48.40	60.66	52.04	71.56
Ga	18.20	19.00	18.37	18.29	18.84
Ge	1.01	0.88	1.00	1.00	1.07
Rb	31.88	29.69	36.76	37.03	29.89
Sr	526.46	540.61	532.17	491.82	420.69
Y	15.15	14.23	13.28	13.52	19.78
Zr	140.43	140.60	130.87	136.76	130.13
Nb	4.61	4.63	4.48	4.61	4.73
Cs	1.51	1.42	1.78	1.97	0.38
Ba	524.67	454.34	499.22	497.89	455.49
La	15.32	14.92	14.53	14.77	15.92
Ce	27.30	28.25	29.74	29.86	31.95
Pr	3.81	3.84	3.53	3.58	4.31
Nd	16.22	16.24	15.05	15.20	17.93
Sm	3.43	3.51	3.14	3.21	4.01
Eu	1.10	1.13	1.07	1.03	1.17
Gd	3.31	3.30	2.75	2.81	3.65
Tb	0.47	0.48	0.42	0.44	0.61
Dy	2.70	2.69	2.36	2.45	3.53
Ho	0.53	0.51	0.46	0.49	0.73
Er	1.55	1.49	1.35	1.38	1.99
Tm	0.23	0.22	0.20	0.21	0.29
Yb	1.47	1.45	1.32	1.34	1.82
Lu	0.23	0.21	0.20	0.20	0.27
Hf	4.02	3.94	3.61	3.82	3.53
Ta	0.36	0.38	0.34	0.36	0.35
Tl	0.32	0.25	0.32	0.34	0.13
Pb	7.21	5.67	6.35	6.37	7.30
Th	3.72	3.74	3.55	3.64	2.72
U	1.24	1.23	1.39	1.23	0.65

Note: Trace elements obtained by fusion ICP-MS.

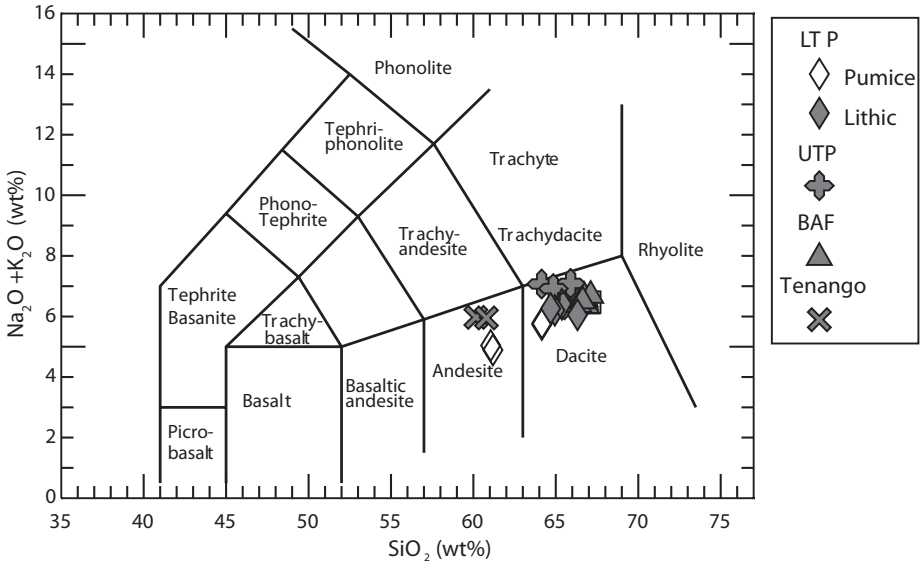

Figure 14. Total alkalies-silica (TAS) classification diagram of pumice and juvenile fragments from the Lower Toluca Pumice (LTP) and other products emitted from the Nevado de Toluca, such as the Upper Toluca Pumice (UTP), block-and-ash flow deposits (BAF), and the 8.5 ka Tenango lava flow belonging to the Chichinautzin volcanic field.

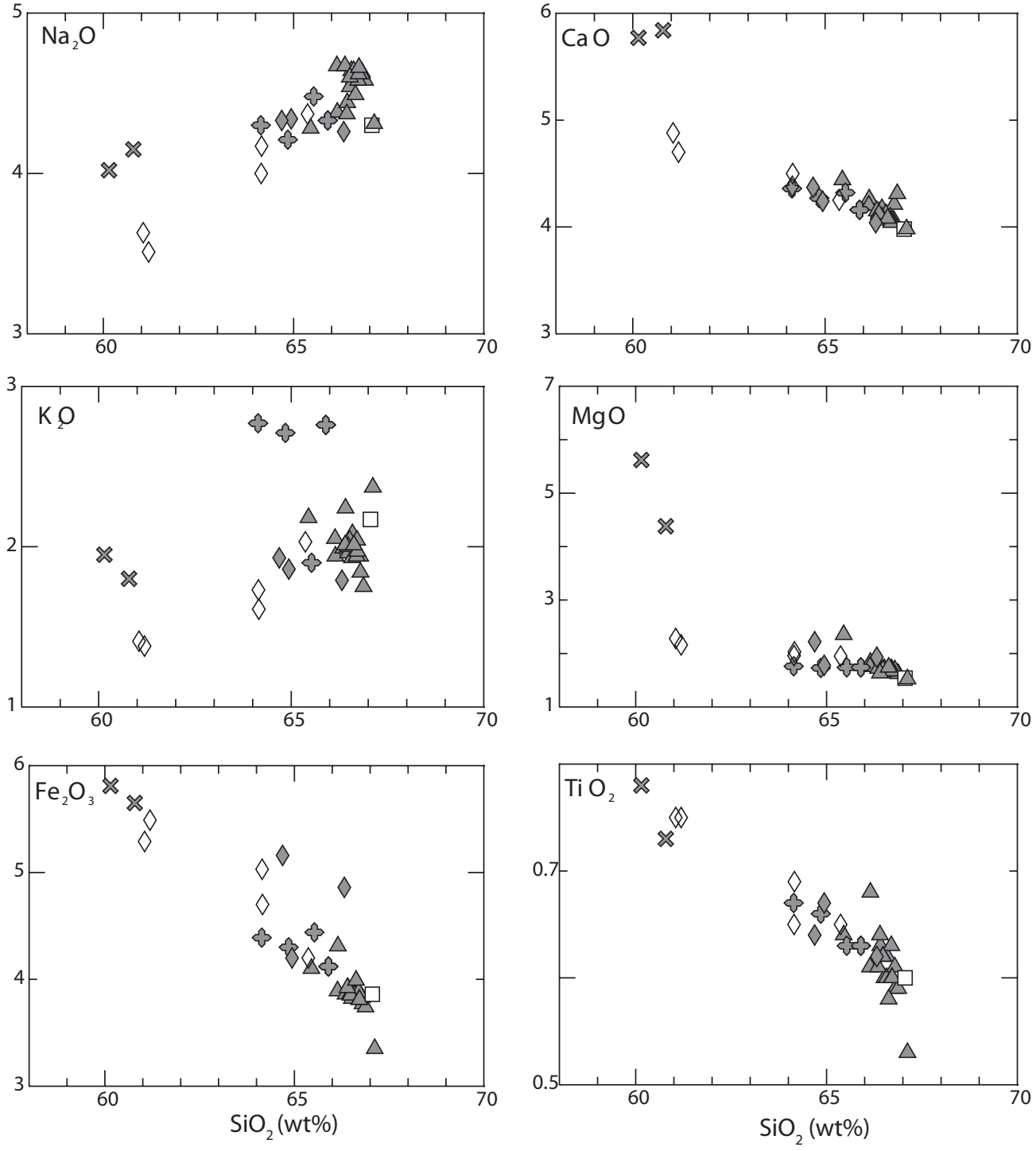

Figure 15. Harker diagrams (all data in wt%) of pumice and juvenile fragments of the Lower Toluca Pumice and other pyroclastic products emitted by Nevado de Toluca volcano. Diamonds—Lower Toluca Pumice (LTP); stars—Upper Toluca Pumice (UTP); triangles—block-and-ash flow deposits (BAF); and crosses—the 8.5 ka Tenango lava flow.

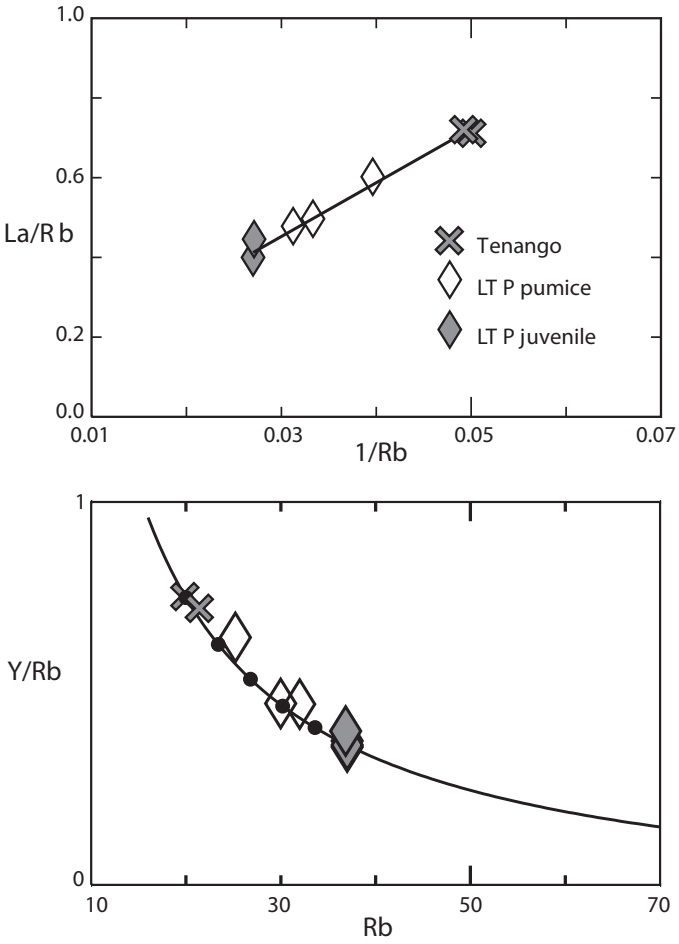

Figure 16. Binary diagrams of 1/Rb versus La/Rb and Rb versus Y/Rb for pumice and juvenile fragments of the Lower Toluca Pumice (LTP) compared with samples from the Tenango lava flow that most likely follow a line of a magmatic mixing process.

ACKNOWLEDGMENTS

This work was supported by CONACYT J-37889T and CNR-CONACYT-SRE grants to Lucia Capra. F. Olmi provided technical support during microprobe analyses performed at CNR Universitá di Firenze, Italy. The ASTER (Advanced Spaceborne Thermal Emission and Reflection Radiometer) satellite image was provided by the U.S. Geological Survey. We are indebted to Lorenzo Vázquez-Selem for the exhaustive review of the first version of the manuscript. Reviews by J. Fierstein and S. de Silva greatly improved the ideas stated in this paper. We also thank B. Martiny, who carefully revised the English grammar of the final manuscript.

REFERENCES CITED

Andersen, D.J., and Lindsley, D.H., 1988, Internally consistent solution models for Fe-Mg-Mn-Ti oxides: Fe-Ti oxides: American Mineralogist, v. 73, p. 714–726.

Arce, J.L., Macías, J.L., and Vázquez-Selem, L., 2003, The 10.5 ka Plinian eruption of Nevado de Toluca volcano, Mexico: Stratigraphy and hazard implications: Geological Society of America Bulletin, v. 115, p. 230–248, doi: 10.1130/0016-7606(2003)115<0230:TKPEON>2.0.CO;2.

Arce, J.L., Cervantes, K.E., Macías, J.L., and Mora, J.C., 2005, The 12.ka Middle Toluca Pumice: A dacitic Plinian–sub-Plinian eruption of Nevado de Toluca in central Mexico: Journal of Volcanology and Geothermal Research, v. 147, p. 125–143, doi: 10.1016/j.jvolgeores.2005.03.010.

Bence, A.E., and Albee, A.L., 1968, Empirical correction factors for the electron microanalysis of silicates and oxides: Journal of Geology, v. 76, p. 382–403.

Bloomfield, K., 1975, A late Quaternary monogenetic volcano field in central Mexico: Geologische Rundschau, v. 64, p. 476–497, doi: 10.1007/BF01820679.

Bloomfield, K., and Valastro, S., 1974, Late Pleistocene eruptive history of Nevado de Toluca volcano, central Mexico: Bulletin of Volcanology, v. 85, p. 901–906.

Bloomfield, K., and Valastro, S., 1977, Late Quaternary tephrochronology of Nevado de Toluca volcano, central Mexico: Overseas Geology and Mineral Resources, v. 46, p. 1–15.

Bloomfield, K., Sánchez Rubio, G., and Wilson, L., 1977, Plinian eruptions of Nevado de Toluca: Geologische Rundschau, v. 66, p. 120–146, doi: 10.1007/BF01989568.

Campa, M.F., and Coney, P., 1983, Tectonostratigraphic terranes and mineral resources distribution in Mexico: Canadian Journal of Earth Sciences, v. 20, p. 1040–1051.

Campa, M.F., Campos, M., Flores, R., and Oviedo, R., 1974, La secuencia mesozoica volcano-sedimentaria metamorfizada de Ixtapan de la Sal, México-Teloloapan, Guerrero: Boletín de la Sociedad Geológica Mexicana, v. 35, p. 7–28.

Capra, L., and Macías, J.L., 2000, Pleistocene cohesive debris flows at Nevado de Toluca volcano, central México: Journal of Volcanology and Geothermal Research, v. 102, p. 149–167, doi: 10.1016/S0377-0273(00)00186-4.

Carey, S., and Sparks, R.S.J., 1986, Quantitative models of the fallout and dispersal of tephra from volcanic eruption columns: Bulletin of Volcanology, v. 48, p. 109–125, doi: 10.1007/BF01046546.

Carey, S.N., Gardner, J.E., and Sigurdsson, H., 1995, Intensity and magnitude of Holocene Plinian eruptions from Mount St. Helens volcano: Journal of Volcanology and Geothermal Research, v. 66, p. 185–202, doi: 10.1016/0377-0273(94)00059-P.

Centeno-García, E., Ruiz, J., Coney, P., Patchett, P.J., and Ortega-Gutierrez, F., 1993, Guerrero terrane of Mexico: Its role in the Southern Cordillera from new geochemical data: Geology, v. 21, p. 419–422, doi: 10.1130/0091-7613(1993)021<0419:GTOMIR>2.3.CO;2.

D'Antonio, M., Capra, L., and Macías, J.L., 2004, Eruptive style and magmatic processes associated to block-and-ash-flow deposits at Nevado de Toluca volcano (Mexico): Petrographic and geochemical evidence: Florence, Italy, 32nd International Geological Congress, p. 403.

De Beni, E., 2001, Evoluzione geologica del vulcano Nevado de Toluca, Messico, analisi stratigrafica petrografica e geochimica [Honor thesis]: Milan, Italy, Universitá degli Studi di Milano, 270 p.

Fierstein, J., and Nathenson, M., 1992, Another look at the calculation of fallout tephra volumes: Bulletin of Volcanology, v. 54, p. 156–167, doi: 10.1007/BF00278005.

Folk, R.L., 1980, Petrology of sedimentary rocks: Austin, Texas, Hemphill, 182 p.

García-Palomo, A., Macías, J.L., Arce, J.L., Capra, L., Espíndola, J.M., and Garduño, V.H., 2002, Geology of Nevado de Toluca volcano and surrounding areas, central Mexico: Geological Society of America Map and Chart Series MCH089.

Gardner, J.E., Rutherford, M., Carey, S., and Sigurdsson, H., 1995, Experimental constraints on pre-eruptive water contents and changing magma storage prior to explosive eruptions of Mount St. Helens volcano: Bulletin of Volcanology, v. 57, p. 1–17.

Heine, K., 1976, Blockgletscher und blockzungen generationen am Nevado de Toluca: Mexiko: Die Erde, v. 107, p. 330–352.

Houghton, B.F., and Wilson, C.J.N., 1989, A vesicularity index for pyroclastic deposits: Bulletin of Volcanology, v. 51, p. 451–462, doi: 10.1007/BF01078811.

Houghton, B.F., Wilson, C.J.N., Del Carlo, P., Coltelli, M., Sable, J.E., and Carey, R., 2004, The influence of conduit processes on changes in style of basaltic Plinian eruptions: Tarawera 1886 and Etna 122 BC: Journal

of Volcanology and Geothermal Research, v. 137, p. 1–14, doi: 10.1016/j.jvolgeores.2004.05.009.

Macías, J.L., García-Palomo, A., Arce, J.L., Siebe, C., Espíndola, J.M., Komorowski, J.C., and Scott, K.M., 1997, Late Pleistocene–Holocene cataclysmic eruptions at Nevado de Toluca and Jocotitlán volcanoes, central Mexico, *in* Kowallis, B.J., ed., Proterozoic to recent stratigraphy, tectonics, and volcanology, Utah, Nevada, southern Idaho and central Mexico: Brigham Young University, Geology Studies, p. 493–528.

Martínez-Serrano, R.G., Schaaf, P., Solís-Pichardo, G., Hernández-Bernal, M.S., Hernández-Treviño, T., Morales-Contreras, J.J., and Macías, J.L., 2004, Sr, Nd, and Pb isotope and geochemical data from the Quaternary Nevado de Toluca volcano, a source of recent adakitic magmatism, and the Tenango volcanic field, Mexico: Journal of Volcanology and Geothermal Research, v. 138, p. 77–110, doi: 10.1016/j.jvolgeores.2004.06.007.

Norini, G., Groppelli, G., Capra, L., and De Beni, E., 2004, Morphological analysis of Nevado de Toluca volcano (Mexico): New insights into the structure and evolution of an andesitic to dacitic stratovolcano: Geomorphology, v. 62, p. 47–61, doi: 10.1016/j.geomorph.2004.02.010.

Sedov, S., Solleiro-Rebolledo, E., Gama-Castro, J.E., Vallejo-Gómez, E., and González-Velázquez, A., 2001, Buried palaeosols of the Nevado de Toluca; an alternative record of late Quaternary environmental change in central Mexico: Journal of Quaternary Science, v. 16, p. 375–389, doi: 10.1002/jqs.615.

Siebe, C., Rodríguez-Lara, V., Schaaf, P., and Abrams, M., 2004, Geochemistry, Sr-Nd isotope composition, and tectonic setting of Holocene Pelado, Guespalapa, and Chichinautzin scoria cones, south of Mexico City: Journal of Volcanology and Geothermal Research, v. 130, p. 197–226, doi: 10.1016/S0377-0273(03)00289-0.

Solleiro-Rebolledo, E., Macías, J.L., Gama-Castro, J.E., Sedov, S., and Sulerzhitsky, L.D., 2004, Quaternary pedostratigraphy of the Nevado de Toluca volcano: Revista Mexicana de Ciencias Geológicas, v. 21, p. 101–109.

Sparks, R.S.J., 1986, The dimensions and dynamics of volcanic eruption columns: Bulletin of Volcanology, v. 48, p. 3–15, doi: 10.1007/BF01073509.

Sparks, R.S.J., Wilson, L., and Hulme, G., 1978, Theoretical modelling of the generation, movement, and emplacement of pyroclastic flows by column collapse: Journal of Geophysical Research, v. 83, p. 1727–1739.

Wilson, C.J.N., and Hildreth, W., 1997, The Bishop Tuff: New insights from eruptive stratigraphy: Journal of Geology, v. 105, p. 407–439.

Wilson, L., Parfitt, E.A., and Head, J.W., 1995, Explosive volcanic eruptions: VIII. The role of magma recycling in controlling the behaviour of Hawaiian-style lava fountains: Geophysical Journal International, v. 121, p. 215–225.

Manuscript Accepted by the Society 28 July 2005

Printed in the USA